NOTATION

A = $\equiv (N_{We})^{1/2}\,[1 + 3(N_{We})^{1/2}\,(N_{Re})^{-1}]$
a = average radius of jet, cm.
d_{ij} = rate of deformation tensor, sec.$^{-1}$
D = diameter of orifice, cm.
g = gravitational constant
H = height of liquid above orifice, cm.
K = viscosity coefficient in Ostwald-de-Waele model, dyne/(sq.cm.)(sec.^{n})
L = unbroken length of the jet, cm.
L_n = unbroken length of Newtonian jet, cm.
L_{nn} = unbroken length of viscoelastic jet, cm.
n = viscosity index in Ostwald-de-Waele model, dimensionless
N_{Re} = Reynolds number, dimensionless = (Du/ν)
N_{We} = Weber number, dimensionless = $(\rho U^2 D/\sigma)$
t = time, sec.
T_b = breakup time, sec.
u_z = velocity in z direction, cm./sec.
u_0 = initial axial velocity, cm./sec.
z = axial direction, cm.

Greek Letters

λ_1 = relaxation time, sec.
ρ = density, g./cu.cm.
σ = surface tension, dyne/cm.
τ_{ij} = stress, dynes/sq.cm.
ν_0 = zero-shear kinematic viscosity, sq.cm./sec.

Subscripts

0 = values based on orifice data
b = values based on data at the breakup point

LITERATURE CITED

1. Kroesser, F. W., and Stanley Middleman, *AIChE J.*, **15**, 383 (1969).
2. Goldin, M., Robert Pfeffer, and Richard Shinnar, paper presented at 62nd Ann. meeting, AIChE, Washington, D. C. (Nov. 1969).
3. Rayleigh, *Proc. Lond. Math. Soc.*, **10**, 7 (1878).
4. Weber, C., *Z. Angew Math. Mech.*, **11**, 136 (1931).
5. Levich, V. G., "Physicochemical Hydrodynamics," Prentice-Hall, Englewood Cliffs, N. J. (1962).
6. Grant, R. P., and Stanley Middleman, *AIChE J.*, **12**, 669 (1966).
7. Fenn, R. W., and Stanley Middleman; *ibid.*, **15**, 379 (1969).
8. Middleman, Stanley, *Chem. Eng. Sci.*, **20**, 1037 (1965).
9. Adamson, A. W., "Physical Chemistry of Surfaces," Wiley, New York (1967).

Manuscript received September 6, 1969; revision received May 1, 1970; paper accepted June 29, 1970.

Tubular Reactor Steady State and Stability Characteristics

C. R. McGOWIN and D. D. PERLMUTTER

School of Chemical Engineering
University of Pennsylvania, Philadelphia, Pa. 19104

I. Effect of Axial Mixing

This paper reports results of a numerical study of the stability characteristics of the nonadiabatic tubular reactor with axial mixing. It differs from much of the prior work on similar systems by its inclusion of a heat transfer term in the modeling equations. Assuming that the tubular reactor with axial mixing (TRAM) has a flat velocity profile, is not packed, and has no radial concentration and temperature gradients, mass and energy conservation statements are, respectively

$$\frac{\partial y}{\partial \tau} = \frac{1}{N_{Pe'}}\frac{\partial^2 y}{\partial z^2} - \frac{\partial y}{\partial z} - \mathcal{R}(y,\eta) \qquad (1)$$

$$\frac{\partial \eta}{\partial \tau} = \frac{1}{N_{Pe}}\frac{\partial^2 \eta}{\partial z^2} - \frac{\partial \eta}{\partial z} + \mathcal{R}(y,\eta) + U_r(\eta_w - \eta) \qquad (2)$$

The commonly used boundary conditions are

$$z = 0, \quad \left.\frac{1}{N_{Pe'}}\frac{\partial y}{\partial z}\right|_0 = y(0) - 1 \qquad (3)$$

$$\left.\frac{1}{N_{Pe}}\frac{\partial \eta}{\partial z}\right|_0 = \eta(0) - \eta_F$$

$$z = 1, \quad \left.\frac{\partial y}{\partial z}\right|_1 = \left.\frac{\partial \eta}{\partial z}\right|_1 = 0 \qquad (4)$$

Correspondence concerning this article should be addressed to Prof. D. D. Perlmutter. C. R. McGowin is with Shell Development Co., P. O. Box 24225, Oakland, California 94623.

Implicit in Equations (1) through (4) is the additional assumption that axial dispersion of mass and energy are described by Fick's law. This model appears to be a reasonable one for many purposes, in spite of the fact that it allows disturbances to be instantaneously propagated upstream. It probably contributes, however, to the effects reported here.

In the steady state condition, Equations (1) and (2) reduce to

$$\frac{1}{N_{Pe'}}\frac{d^2y}{dz^2} - \frac{dy}{dz} - \mathcal{R}(y,\eta) = 0 \tag{5}$$

$$\frac{1}{N_{Pe}}\frac{d^2\eta}{dz^2} - \frac{d\eta}{dz} + \mathcal{R}(y,\eta) + U_r(\eta_w - \eta) = 0 \tag{6}$$

The earlier emphasis on study of the adiabatic case arose from the fact that Equations (5) and (6) may be uncoupled for $U_r = 0$ and $N_{Pe'} = N_{Pe}$. As a consequence of this major simplification, techniques that are applicable only to systems described by single differential equations could be used to perform the steady state and stability analysis. Van Heerden (*18*) and Raymond and Amundson (*15*) used an integral technique to determine the number and locations of the steady states. Using Sturm's oscillation theorems, Amundson (*1*) derived a necessary and sufficient condition for local stability that does not require evaluation of the dominant eigenvalue of the linearized unsteady state equation. Luss and Amundson (*8*) and Luss (*10*) used topological methods to derive sufficient conditions for the uniqueness of the steady state. Other investigators have also studied the adiabatic case but used techniques not necessarily restricted to that case. Among these are Chiou and Cohen (*4*), who studied the frequency response of the linearized system, and Berger and Lapidus (*2*), who derived a sufficient condition for local stability using the Liapunov functional method.

The results to be presented in this paper are developed by a technique general enough to handle the coupled equations. To make the findings more compatible with prior work in the field, it is assumed that the axial mass and thermal diffusivities are equal, and that the single chemical reaction is first order, irreversible, and has Arrhenius temperature dependence:

$$\mathcal{R}(y,\eta) = k_0 \quad e^{-\gamma/\eta}\, y \tag{7}$$

THE METHODS OF ANALYSIS

The TRAM was systematically investigated by first generating steady state operating curves, showing reactant concentration at the reactor exit as functions of the feed temperature for various combinations of the wall heat transfer coefficient and the Peclet numbers. Subsequently, boundaries of the regions of instability were located on these curves by using Galerkin's method to determine the local stability character of the steady states.

The detailed computations required numerical solution of Equations (5) and (6) with boundary conditions (3) and (4) for a wide range of values of η_F and $y(1)$. The solution of this nonlinear two-point boundary-value problem was carried out using the Newton-Raphson procedure (*11*) in conjunction with backward integration from $z = 1$ to $z = 0$. Two different methods, which are described by Reilly and Schmitz (*16*), were used to obtain discrete points on the steady state operating curves.

In Method 1 the feed temperature is fixed, and the Newton-Raphson method is used to solve for the exit concentration and temperature that yield steady state profiles satisfying the boundary conditions at $z = 0$. In Method 2 the exit reactant concentration is fixed, and the Newton-Raphson method is used to solve for the exit temperature that yields a steady state concentration profile that satisfies the boundary condition on y at $z = 0$. When the iterative Newton-Raphson computation converges, the boundary condition on η at $z = 0$ is rearranged to solve for the feed temperature:

$$\eta_F = \eta(0) - \frac{1}{N_{Pe}}\frac{d\eta}{dz}\bigg|_0 \tag{8}$$

Method 2 was used to compute steady states located on the steeply sloped and positively sloped portions of the steady state operating curves, where $y(1)$ is very sensitive to small changes in the feed temperature, while Method 1 was used to compute the remaining steady states. Method 2 requires fewer computations than Method 1, since $\eta(1)$ is the only unknown in Method 2 and both $y(1)$ and $\eta(1)$ are unknowns in Method 1. Method 1 was used only when it was necessary to generate steady state profiles for a given value of the feed temperature or when the sensitivity of $y(1)$ to η_F was low.

After each steady state operating curve had been generated, the local stability character of the steady states was determined, using Galerkin's method to estimate the dominant eigenvalue of the linearized equations:

$$\frac{\partial \hat{y}}{\partial \tau} = \frac{1}{N_{Pe'}}\frac{\partial^2 \hat{y}}{\partial z^2} - \frac{\partial \hat{y}}{\partial z} - \mathcal{R}_y(z)\hat{y} - \mathcal{R}_\eta(z)\hat{\eta} \tag{9}$$

$$\frac{\partial \hat{\eta}}{\partial \tau} = \frac{1}{N_{Pe}}\frac{\partial^2 \hat{\eta}}{\partial z^2} - \frac{\partial \hat{\eta}}{\partial z} + \mathcal{R}_y(z)\hat{y} + (\mathcal{R}_\eta(z) - U_r)\hat{\eta} \tag{10}$$

$$z = 0: \quad \frac{1}{N_{Pe'}}\frac{\partial \hat{y}}{\partial z}\bigg|_0 = \hat{y}(0), \quad \frac{1}{N_{Pe}}\frac{\partial \hat{\eta}}{\partial z}\bigg|_0 = \hat{\eta}(0) \tag{11}$$

$$z = 1: \quad \frac{\partial \hat{y}}{\partial z}\bigg|_1 = \frac{\partial \hat{\eta}}{\partial z}\bigg|_1 = 0 \tag{12}$$

The application of Galerkin's method reduces Equations (9) and (10) to an approximately equivalent set of $2m$ linear ordinary differential equations, which can be written in the following matrix-vector notation:

$$\frac{d\mathbf{x}}{d\tau} = \mathbf{A}\,\mathbf{x} \tag{13}$$

Since the procedure and the resulting reduced system are given in a previous paper (*13*), the details are not discussed here.

The vector $\mathbf{x}$ in Equation (13) is composed of the undetermined coefficients in the trial solutions for $\hat{y}$ and $\hat{\eta}$:

$$\mathbf{x}^T = [a_1\ a_2 \ldots a_m\ \ b_1\ b_2 \ldots b_m]$$

The necessary and sufficient condition for local stability is that the dominant eigenvalue of the matrix $\mathbf{A}$ converges to a constant value with negative real part as the number of terms in the trial solutions increases. If the dominant eigenvalue converges to a value having positive real part, the steady state is unstable. The boundary of the region of instability in the graph of the steady state operating curves is the locus of marginally stable steady states. In another paper (*13*), it was shown that estimates of the dominant eigenvalue for the TRAM system, obtained using

Galerkin's method, converge monotonically in the positive direction.

NUMERICAL RESULTS

Steady state operating curves and the associated regions of instability were generated for various combinations of the wall heat transfer coefficient and the axial Peclet numbers. For ease of comparison, the dimensionless parameters

$$k_0' = 1.0 \times 10^{11}, \quad \gamma = 75, \quad \text{and} \quad \eta_w = 2.50$$

were taken directly from Reilly and Schmitz' analysis of the plug-flow tubular reactor with recycle (*16*). The results for $N_{Pe} = 10$ and a range of values of U_r are shown in Figures 1 and 2, the latter on semilogarithmic coordinates to expand the low conversion region. Figures 3 and 4 show steady state operating curves for the limiting cases of the TRAM: $N_{Pe} = 0$ (infinite axial mixing) and $N_{Pe} = \infty$ (zero axial mixing), which correspond to the continuous stirred-tank reactor (CSTR) and the plug-flow tubular reactor (PFTR), respectively (*7, 12*). In Figure 5 the TRAM steady state operating curves are plotted for $U_r = 0.10$ and for discrete values of the axial Peclet numbers between zero and infinity.

The operating curves for $N_{Pe} = 0$ in Figure 3 were obtained by solving the steady state balances for the equivalent CSTR system:

$$1 - y - k_0' e^{-\gamma/\eta} y = 0 \tag{14}$$

$$\eta_F - \eta + U_r(\eta_w - \eta) + k_0' e^{-\gamma/\eta} y = 0 \tag{15}$$

The necessary and sufficient condition for local instability is that both of the following inequalities are satisfied at steady state conditions (3):

$$(1 + U_r) > \left[\frac{K}{(1+K)^2} \frac{\gamma}{\eta^2} \right] \tag{16}$$

$$(1 + U_r) > (1 + K) \left[\left(\frac{K}{(1+K)^2} \frac{\gamma}{\eta^2} \right) - 1 \right] \tag{17}$$

The steady state operating curves for $N_{Pe} = \infty$ in Figure 4 were generated using the Runge-Kutta method to integrate the steady state material and energy balances of

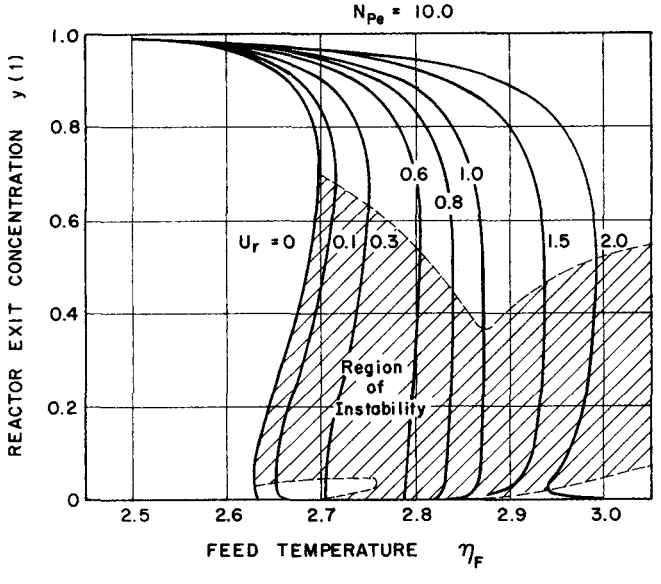

Fig. 1. Steady state operating curves for the TRAM.

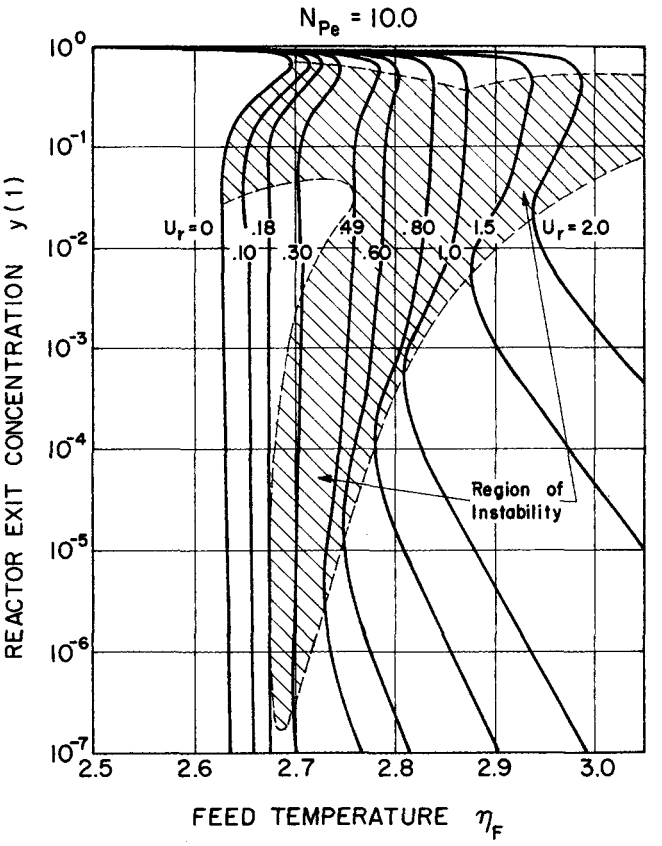

Fig. 2. Steady state operating curves for the TRAM on expanded ordinate scale.

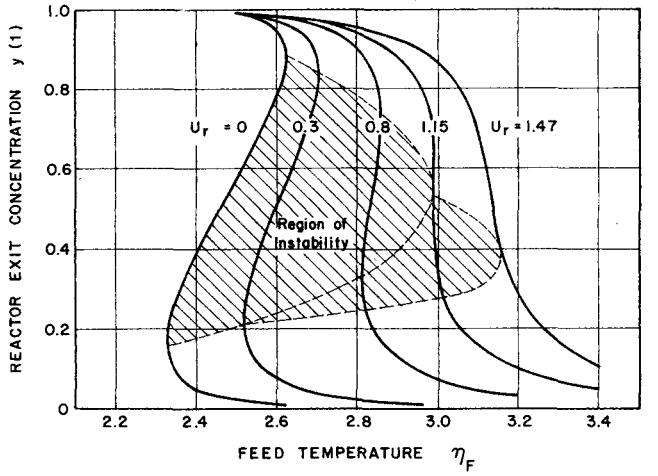

Fig. 3. Steady state operating curves for the CSTR; limiting case of the TRAM for $N_{Pe} = 0$.

the equivalent PFTR system:

$$\frac{dy}{dz} = -k_0' e^{-\gamma/\eta} y \tag{18}$$

$$\frac{d\eta}{dz} = U_r(\eta_w - \eta) + k_0' e^{-\gamma/\eta} y \tag{19}$$

$$z = 0: \quad y(0) = 1, \quad \eta(0) = \eta_F \tag{20}$$

Since no axial feedback of mass or energy is present in the PFTR system, only unique, globally asymptotically stable steady states can exist (*18*). Thus no region of instability exists in this case.

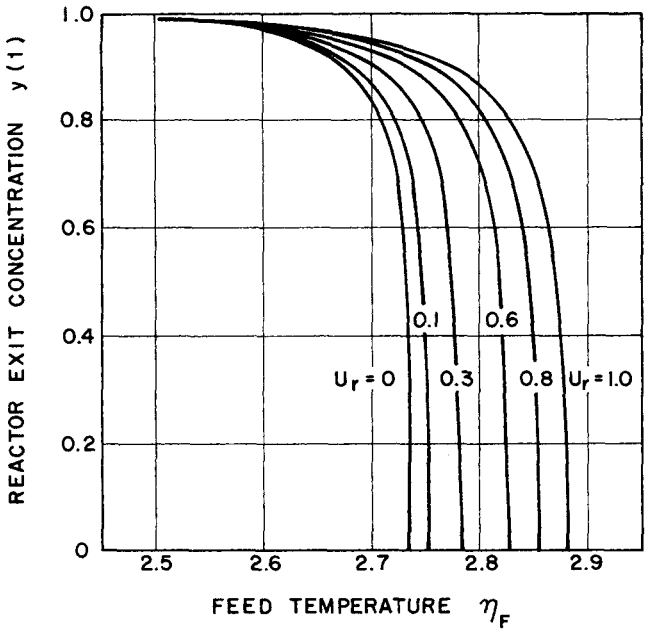

Fig. 4. Steady state operating curves for the PFTR; limiting case of the TRAM for $N_{Pe} = \infty$.

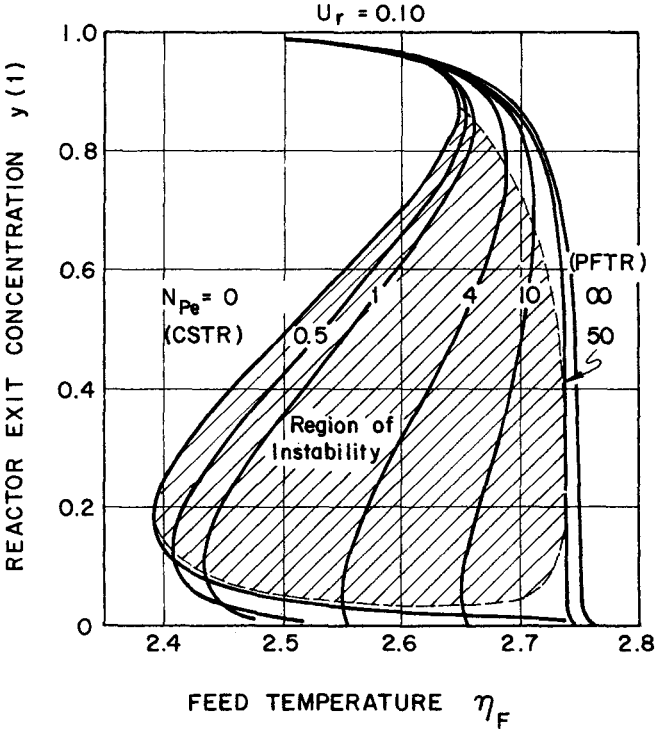

Fig. 5. Steady state operating curves for the TRAM.

For intermediate values of the Peclet number, the TRAM operating curves were generated using the Newton-Raphson method in conjunction with Runge-Kutta numerical integration of Equations (5) and (6) and the Newton-Raphson auxiliary equations from $z = 1$ to $z = 0$. A grid of 200 equal increments was used in the Runge-Kutta integrations. The Newton-Raphson convergence constant was 10^{-12} in the calculation of high conversion steady states and 10^{-6} for the others, and double precision arithmetic was used to compute most of the steady states. The Newton-Raphson solution of the two-point boundary-value problem usually converged within five iterations; however, Newton-Raphson Method 1 would not converge to steady states located on positively sloped portions of the steady state operating curves, and it was necessary to use Method 2 to compute these steady states.

In the Galerkin analysis of local stability, 16 terms were used in the trial solutions to determine the local stability character of low conversion steady states, and 24 terms were used for high conversion steady states. The eigenvalues of the matrix A in Equation (13) were computed using the QR method (5), an iterative technique involving successive unitary transformations of A.

DISCUSSION

Except for the operating curves for the limiting case, $N_{Pe} = \infty$, each set of TRAM operating curves shows that multiple steady states are possible over a wide range of wall heat transfer coefficients and Peclet numbers; that is, for some operating curves, there is a range of feed temperatures, $\eta_{min} < \eta_F < \eta_{max}$, over which multiple steady states exist and outside of which only unique steady states exist. For the various members of the family of operating curves, the upper and lower bounds of this range of feed temperatures determine the locus of maximum and minimum feed temperatures (locus of MMFT). This locus coincides with the boundary of the regions of instability in Figures 1, 2, and 5 and is the larger of the two parabolically shaped broken lines in Figure 3.

Steady State Operating Curves

The unusual shape of the lower part of the locus of MMFT in Figures 1 and 2 indicates that there is a range of wall heat transfer coefficients in which as many as five steady states exist. The lower part of the locus of MMFT doubles back on itself and is tangent to the steady state operating curves for $U_r = 0.18$ and $U_r = 0.49$. For heat transfer coefficients inside this range, the locus of MMFT crosses the operating curve four times, and one, three, or five steady states exist. In order to clarify the relation between the locus of MMFT and the steady state operating curves for values of U_r in this range, a hypothetical operating curve is plotted in Figure 6 which exaggerates the properties of the curve for $U_r = 0.30$ of Figure 2. Two sets of relative maximum and minimum feed temperatures exist for this operating curve, and these are identified in Figure 6. Multiple steady states occur for $\eta_{min_2} < \eta_F < \eta_{max_1}$, and only unique steady states exist otherwise. Thus of the five feed temperatures that are marked in Figure 6, η_{F_1} and η_{F_5} correspond to systems having unique steady states, while η_{F_2}, η_{F_3}, and η_{F_4} correspond to systems having multiple steady states. Further examination of Figure 6 shows that five steady states exist when $\eta_{min_1} < \eta_F < \eta_{max_2}$ and three steady states exist when $\eta_{min_2} < \eta_F < \eta_{min_1}$ or $\eta_{max_2} < \eta_F < \eta_{max_1}$.

The relative minimum and maximum feed temperatures from the steady state operating curve corresponding to $N_{Pe} = 10$ and $U_r = 0.40$ are

$$\eta_{min_2} = 2.7164$$

$$\eta_{min_1} = 2.7336$$

$$\eta_{max_2} = 2.7341 \quad \text{and} \quad \eta_{max_1} = 2.7679$$

Consequently, multiple steady states exist for $2.7164 < \eta_F < 2.7679$, which corresponds to a range of 5°K. for a typical set of system parameters (12). Five steady states exist for $2.7336 < \eta_F < 2.7341$, which corresponds to a range of only 0.05°K. Thus it would be difficult to obtain a system having five steady states for the parameters used in this paper, since random variations of the feed temperature would be expected to exceed 0.05°K.

Hatfield and Aris (6) examined the steady state operating characteristics of the catalyst particle with finite mass and energy transport both inside the particle and between the particle surfaces and its surroundings. This system has the same boundary conditions as the tubular reactor with axial mixing. The authors found that in some cases as many as five steady states exist for a limited range of the Thiele modulus, and they noted that if the rates of mass and energy transport are infinite either inside the particle or between the particle surface and its surroundings, then a maximum of only three steady states is possible. This suggests that if the concentration and temperature are set equal to the feed stream conditions in the TRAM system instead of being constrained by the boundary conditions given in Equation (3), it would not be possible to obtain five steady states. Thus the five-steady state phenomenon appears to be a property of the mathematical model and not necessarily a property of tubular reactors in practice.

Additional steady state operating curves, generated for $U_r = 3.0$ and 4.0, but not plotted in Figures 1 and 2, demonstrate that multiple steady states are possible in the TRAM system for heat transfer coefficients up to at least 4.0 when $N_{Pe} = 10$.

The boundary of the region of instability in Figures 1 and 2 coincides with the locus of maximum and minimum feed temperatures, indicating that (1) unique steady states are locally stable; (2) in systems having three steady states, the intermediate steady state is unstable and therefore unattainable without external feedback control, while the low and high temperature steady states are locally stable; and (3) the first, third, and fifth steady states of systems having five steady states are locally stable, while the second and fourth are unstable. For $U_r = 3.0$, however, local stability analysis of steady states located just below the lower part of the locus of MMFT showed that the locus of marginal stability no longer coincides with the locus of MMFT but encloses the high conversion steady state of some systems having three steady states. In such cases, the high conversion steady state is unstable, making the low conversion steady state the only stable one present.

The steady state operating curves and the associated region of instability of Figure 5 show that the TRAM exhibits a uniform transition between the properties of the CSTR and those of the PFTR as the degree of axial mixing varies between its two limits. One or three steady states exist for Peclet numbers less than about 50, and only unique steady states exist otherwise. Unique steady states are locally stable, while in systems having three steady states, the low and high conversion steady states are locally stable, and the intermediate steady state is unstable.

Ignition and Extinction Temperatures

The feed temperatures corresponding to the upper and lower points of intersection between the locus of marginal stability and the steady state operating curve under consideration are the ignition temperature and the extinction temperature of the system, respectively. If the locus of marginal stability coincides with the locus of MMFT, the ignition and extinction temperatures are equal to the relative maximum and minimum feed temperatures, respectively.

When five steady states are present in the TRAM system, it may be difficult to ever attain the intermediate stable steady state. For example, with reference to Figure 6, a reactor operating at high conversion steady state 5 would shift to a low conversion steady state if the feed temperature were to decrease to a level below η_{min_2}. On the other hand, a feed temperature increase beyond η_{max_1} would shift the reactor back to a high conversion steady state. Intermediate steady state 3 can only be reached by inducing a positive temperature disturbance and negative concentration disturbance from steady state 1 (or disturbances of the opposite signs from steady state 5) of such magnitudes that the reactor shifts to steady state 3. In effect, this system will usually behave as if it has only two stable steady states.

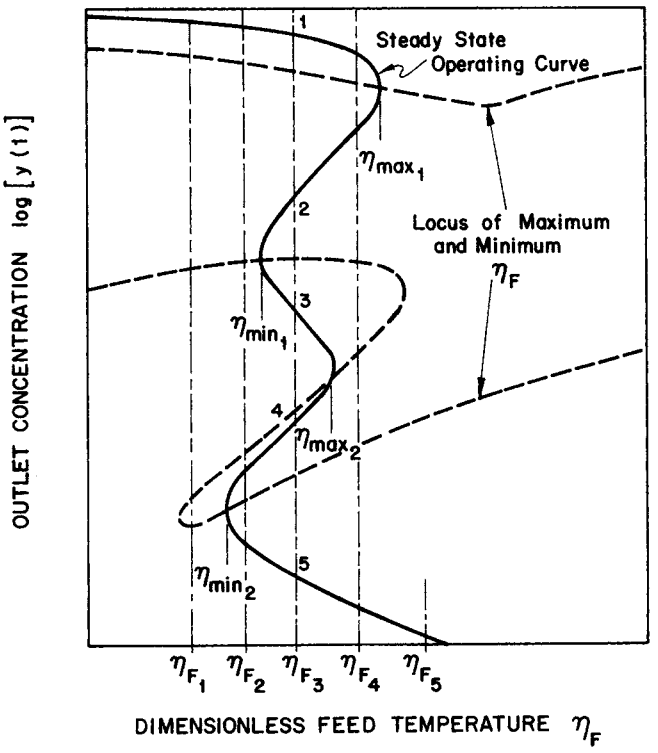

Fig. 6. Hypothetical steady state operating curve for the TRAM.

The CSTR Limiting Case

The CSTR curves of Figure 3 are similar to those computed by Reilly and Schmitz for the PFTR-recycle system (16). As the wall heat transfer coefficient increases, the transitions between multiple steady state and unique steady state behavior and those between unstable and stable behavior occur in the same sequence in both systems. The common characteristic of these two systems is that a significant degree of axial feedback of mass and energy exists in each case, via internal backmixing in the CSTR and external recycle in the PFTR-recycle system. In particular, the CSTR possesses either a unique and locally stable steady state or two locally stable and one unstable steady state for $0 \leq U_r < 0.30$. For $0.30 \leq U_r < 1.15$, the high conversion steady state of systems having three steady states may be unstable since the locus of marginal stability has separated from the locus of MMFT. In the range $1.15 \leq U_r < 1.47$, only unique steady states are possible, of which some are unstable and exhibit limit cycle or continuous oscillations of the concentration and temperature about the equilibrium point. Unique unstable steady states are also possible for heat transfer coefficients slightly less than 1.15. For $U_r \geq 1.47$, only unique, locally stable steady states exist.

The locus of MMFT and the locus of marginal stability in Figure 3 were generated by transforming inequalities (16) and (17) into equalities:

$$(1 + U_r) = \frac{K}{(1+K)^2}\,\frac{\gamma}{\eta^2} = L_1 \qquad (21)$$

$$(1 + U_r) = (1 + K)\left[\left(\frac{K}{(1+K)^2}\,\frac{\gamma}{\eta^2}\right) - 1\right] = L_2 \qquad (22)$$

and solving for the values of U_r at the various temperature levels η. The feed temperature and reactant concentration corresponding to each combination of η and U_r were obtained using the expressions

$$\eta_F = (1 + U_r)\eta - U_r\eta_w - K/(1 + K) \qquad (23)$$

$$y = 1/(1 + K) \qquad (24)$$

The boundary of the region of instability is given by the outer boundary of the area enclosed within the two curves of y versus η_F that result.

The values of U_r beyond which only unique steady states and only locally stable steady states occur can be determined directly by graphing the functions L_1 and L_2, as shown in Figure 7. The maximum value of L_1 is $(1 + U_r) = 2.15$ and occurs at $\eta = 2.947$. The maximum value of L_2 is $(1 + U_r) = 2.47$ and occurs at $\eta = 3.017$. Hence inequality (16) cannot be violated for $U_r > 1.15$, and all steady states are then unique. Similarly, inequality (17) is always satisfied for $U_r > 1.47$, and all steady states are then locally stable. The points at which the locus of MMFT and the locus of marginal stability separate in Figure 3 correspond to those values of U_r at which the functions L_1 and L_2 are equal in Figure 7; that is, $U_r = 0.30$ and $U_r = 1.15$.

Since the CSTR represents one of the limiting cases of the TRAM system as axial mixing varies, it is reasonable to expect that the TRAM will exhibit the same characteristic progression of the steady state operating curves as the CSTR as the heat transfer coefficient increases, at least when the degree of axial mixing is large. Hence, it may be expected that the TRAM will exhibit limit cycle behavior when the heat transfer coefficient is increased beyond the range covered in this study. Available data for overall heat transfer coefficients in tubular heat exchangers (*14*) indicate, however, that practical values of the wall heat transfer coefficient fall within the range investigated here for the TRAM system ($0 \leq U_r < 4.0$) and within and beyond the range in which multiple and unstable steady states are possible in the CSTR ($0 \leq U_r < 1.47$).

An important aspect of the steady state operating characteristics of the TRAM is that multiple steady states are possible over a much wider range of wall heat transfer coefficients (for $N_{Pe} = 10$) than for either the CSTR or the PFTR.

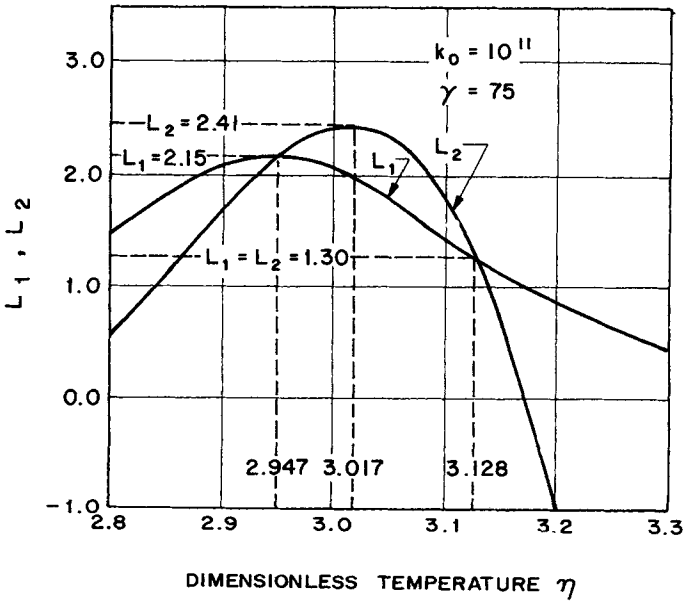

Fig. 7. Functions that provide conditions for stability of the CSTR.

ACKNOWLEDGMENT

The authors gratefully acknowledge the support of the National Aeronautics and Space Administration, the family of Wilson S. Yerger, the National Science Foundation, and a University of Pennsylvania Computer Center grant of funds for computer time. Professor S. W. Churchill was most helpful as an interim advisor during Daniel D. Perlmutter's sabbatical leave.

NOTATION

$\mathbf{A}$ = matrix as defined in Equation (13)
C = reactant concentration, g.-mole/cc.
C_p = fluid heat capacity, cal./(g.)(°K.)
D = effective mass diffusivity, sq.cm./sec.
E = activation energy, cal./g.-mole
$(-\Delta H_r)$ = heat of reaction, cal./g.-mole
k = thermal conductivity of fluid, cal./(sq.cm.)(sec.)(°K.)(cm.)
k_0 = frequency factor, sec.$^{-1}$
k_0' = dimensionless frequency factor (k_0L/v)
K = $k_0'\,e^{-\gamma/\eta}$
L = reactor length, cm.
L_1, L_2 = functions as defined in Equations (21) and (22)
m = number of terms in trial solutions in Galerkin stability analysis
N_{Pe} = heat transfer Peclet number (vL/α)
$N_{Pe'}$ = mass transfer Peclet number (vL/D)
R = gas constant, 1.987 cal./(g.-mole)(°K.)
R' = reactor tube radius, cm.
$\mathcal{R}(y, \eta)$ = dimensionless reaction rate
$\mathcal{R}_y(z) = \partial\mathcal{R}(y, \eta)/\partial y|_{ss}$
$\mathcal{R}_\eta(z) = \partial\mathcal{R}(y, \eta)/\partial\eta|_{ss}$
t = time, sec.
T = temperature, °K.
U = wall heat transfer coefficient, cal./(sq.cm.)(sec.)(°K.)
U_r = dimensionless wall heat transfer coefficient $(2UL/\rho C_pR'v)$
v = flow velocity, cm./sec.
x = axial position, cm.
$\mathbf{x}$ = vector as defined in Equation (13)
y = dimensionless concentration (C/C_F)
z = dimensionless axial position (x/L)

Greek Letters

α = thermal diffusivity, $(k/\rho C_p)$
γ = dimensionless activation energy $(\rho C_pE/(-\Delta H_r)C_FR)$
η = dimensionless temperature $(\rho C_pT/(-\Delta H_r)C_F)$
ρ = fluid density, g./cc.
τ = dimensionless time (vt/L)

Superscript

$\wedge$ = disturbance from steady state condition

Subscripts

F = evaluated at feed stream conditions
ss = evaluated at steady state conditions
w = evaluated at reactor wall conditions

LITERATURE CITED

1. Amundson, N. R., *Can. J. Chem. Eng.*, **43**, 49 (1965).
2. Berger, A. J., and Leon Lapidus, *AIChE J.*, **14**, 558 (1968).
3. Bilous, O., and N. R. Amundson, *ibid.*, **1**, 513 (1955).
4. Chiou, J. K. S., and W. C. Cohen, paper presented at AIChE,, St. Louis meeting (1968).
5. Francis, J. G. F., *Computer J.*, **4**, 265, 332 (1961).
6. Hatfield, B., and Rutherford Aris, *Chem. Eng. Sci.*, **24**, 1213 (1969).
7. Levenspiel, O., "Chemical Reaction Engineering," Wiley, New York (1962).
8. Luss, D., and N. R. Amundson, *Chem. Eng. Sci.*, **22**, 253 (1967).
9. ———, *Can. J. Chem. Eng.*, **45**, 341 (1967).
10. Luss, D., *Chem. Eng. Sci.*, **23**, 1249 (1968).
11. McGinness, P. H., Jr., *Chem. Eng. Progr. Symp. Ser. No. 55*, **61** (1959).
12. McGowin, C. R., Ph.D. dissertation, Univ. Pennsylvania, Philadelphia (1969).
13. ———, and D. D. Perlmutter, *AIChE J.*, **17**, 837 (1971).
14. Perry, J. H., ed., "Chemical Engineers' Handbook," 4th edit., McGraw-Hill, New York (1963).
15. Raymond, L. R., and N. R. Amundson, *Can. J. Chem. Eng.*, **42**, 173 (1964).
16. Reilly, M. J., and R. A. Schmitz, *AIChE J.*, **12**, 153 (1966).
17. Van Heerden, C., *Ind. Eng. Chem.*, **45**, 1242 (1953).
18. ———, *Chem. Eng. Sci.*, **8**, 133 (1958).
19. Wehner, J. F., and Wilhelm, R. H., *ibid.*, **6**, 89 (1956).

II. Limiting Behavior and Collocation Solution of the Radial Mixing Case

A tubular reactor model that accounts for both radial gradients and nonflat velocity profile is unusually difficult to solve numerically, since even the steady state energy and material balances of the system are ordinarily coupled nonlinear partial differential equations. Nevertheless, techniques have been developed to obtain approximate or special-case analytical solutions. Kramers and Westerterp (*8*), von Rosenberg, Durrill, and Spencer (*14*), and Mickley and Letts (*11, 12*) used implicit finite-difference techniques to obtain direct numerical solutions. Hsu (*6*) obtained the analytical series solution of the material balance for the isothermal tubular reactor with finite radial mixing, parabolic velocity profile, first-order chemical reaction, and no axial diffusion, by reducing the system to an eigenvalue problem. The Taylor axial diffusion model (*1, 3, 15*) combines the effects of axial diffusion, radial concentration gradients, and parabolic velocity profile into a single axial diffusion term, reducing the steady state material balance for the isothermal system to a second-order ordinary differential equation. Deans and Lapidus (*4*) devised a two-dimensional array of interconnected continuous stirred-tank reactors to approximate the behavior of the packed-bed tubular reactor, and McGuire and Lapidus (*10*) used this model in an extensive numerical study to simulate the transient response of the system.

The model for the tubular reactor with finite radial mixing (TRRM) assumes that the velocity profile is flat, that axial diffusivity and conductivity are zero, and that heat transfer occurs across the reactor wall. The dimensionless steady state material and energy balances are

$$\frac{\partial y}{\partial z} = \frac{1}{N_{Pe'}} \frac{1}{r} \frac{\partial}{\partial r}\left[r \frac{\partial y}{\partial r} \right] - \mathcal{R}(y, \eta) \qquad (1)$$

$$\frac{\partial \eta}{\partial z} = \frac{1}{N_{Pe}} \frac{1}{r} \frac{\partial}{\partial r}\left[r \frac{\partial \eta}{\partial r} \right] + \mathcal{R}(y, \eta) \qquad (2)$$

and the boundary conditions are

$$z = 0: \quad y(0, r) = 1, \quad \eta(0, r) = \eta_F \qquad (3)$$

$$r = 0: \quad \left.\frac{\partial y}{\partial r}\right|_0 = \left.\frac{\partial \eta}{\partial r}\right|_0 = 0 \qquad (4)$$

$$r = 1: \quad \left.\frac{\partial y}{\partial r}\right|_1 = 0, \quad \left.\frac{1}{N_{Pe}} \frac{\partial \eta}{\partial r}\right|_1 = U_r [\eta_w - \eta(1)] \qquad (5)$$

These boundary conditions assume flat radial concentration and temperature profiles at the reactor entrance and no mass transfer across the reactor wall. In the absence of radial velocity gradients, radial variations of concentration and temperature result from finite resistances to radial mass and heat transfer. Thus the radial heat and mass transfer Peclet numbers, N_{Pe} and $N_{Pe'}$, are computed using the thermal and mass diffusivities for the reactant mixture.

In the following, a direct comparison will be made of the collocation and implicit finite-difference techniques for obtaining solutions of Equations (1) and (2) numerically. In addition, limiting forms of this model will be explored analytically for both extremes of the degree of radial mixing.

LIMITING BEHAVIOR

As radial dispersive effects approach either zero or infinity in the tubular reactor system, the radial gradients of concentration and temperature must disappear when the entrance profiles and the velocity profiles are flat. This occurs at the zero mixing extreme, because there is no mechanism by which the uniform reaction effects can be